

Optical transitions in broken gap heterostructures

E. Halvorsen*

Department of Physics, P.O. Box 1048 Blindern, N-0316 Oslo, Norway

Y. Galperin

Department of Physics, P.O. Box 1048 Blindern, N-0316 Oslo, Norway

and Division of Solid State Physics, Ioffe Physico-Technical Institute of Russian Academy of Sciences, 194021 St. Petersburg, Russia

K. A. Chao

Department of Physics, Lund University, Sölvegatan 14A, S-223 62 Lund, Sweden

(Received 4 October 1999)

We have used an eight-band model to investigate the electronic structures and to calculate the optical matrix elements of InAs-GaSb broken gap semiconductor heterostructures. The unusual hybridization of the conduction band states in the InAs layers with the valence band states in the GaSb layers has been analyzed in detail. We have studied the dependence of the optical matrix elements on the degree of conduction-valence hybridization, the tuning of the hybridization by varying the width of the GaSb layers and/or InAs layers, and the sensitivity of quantized levels to this tuning. Large spin-orbit splitting in the energy bands has been demonstrated. Our calculation can serve as a theoretical model for infrared lasers based on broken gap quantum well heterostructures.

I. INTRODUCTION

The characteristic feature of $\text{Al}_x\text{Ga}_{1-x}\text{Sb}/\text{InAs}$ heterostructures with $x < 0.3$ is the overlap of the InAs conduction band with the $\text{Al}_x\text{Ga}_{1-x}\text{Sb}$ valence band.¹ Such systems, often referred to as *broken gap* heterostructures, exhibit interesting negative persistent photoconductivity,² a semimetal-semiconductor transition induced by a magnetic field,³ and intrinsic exciton.⁴ As the Al concentration increases from $x = 0.3$, a staggered band alignment appears at the $\text{Al}_x\text{Ga}_{1-x}\text{Sb}/\text{InAs}$ interface with the valence band edge of $\text{Al}_x\text{Ga}_{1-x}\text{Sb}$ lying in the band gap of InAs. On the other hand, at a GaSb/ $\text{Al}_x\text{Ga}_{1-x}\text{Sb}$ interface the band alignment is of the straddled type. Therefore, in a InAs/ $\text{Al}_x\text{Ga}_{1-x}\text{Sb}/\text{GaSb}$ heterostructure, carriers can tunnel from the InAs conduction band to the GaSb valence band through the $\text{Al}_x\text{Ga}_{1-x}\text{Sb}$ barrier.

InAs, GaSb, and AlSb form a family of semiconductors with sufficient lattice match for epitaxial growth. Interband tunneling devices based on InAs/ $\text{Al}_x\text{Ga}_{1-x}\text{Sb}/\text{GaSb}$ double-barrier resonant tunneling have been fabricated, which exhibit high frequency response and peak-to-valley current ratio at room temperatures.⁴⁻¹² Because of their potential for technological applications,¹³ resonant tunneling¹⁴⁻¹⁶ and resonant magnetotunneling¹⁷⁻²⁰ have been investigated extensively.

In contrast to tunneling processes, very little work has been done on the electronic structure and optical properties of broken gap heterostructures.²¹⁻²³ We note that due to the overlap of the InAs conduction band and the GaSb valence band, it is possible to form different type of eigenstate with interesting optical properties. We demonstrate this with Fig. 1 where the conduction band edge E_c and the valence band edge E_v are marked for a GaSb/InAs heterostructure embedded in the band gap of AlSb. Treating the AlSb at both sides

as a potential barrier, the system AlSb/GaSb/InAs/AlSb is essentially a type of quantum well, which we call a broken gap quantum well (BGQW). If we diminish the thickness of either the GaSb layer or the InAs layer to zero, the BGQW is reduced to a conventional quantum well which with bipolar doping becomes a quantum well laser.

If in a properly designed BGQW there exist two eigenenergies as shown in Fig. 1, under bipolar doping the BGQW can lase in the infrared frequency region. Such semiconductor infrared lasers or detectors were proposed earlier.^{24,25} The lower energy state in Fig. 1 is characterized by the degree of hybridization between the GaSb valence band states and the InAs conduction band states. Enhancement of the optical transition requires the hybridized wave function to have a

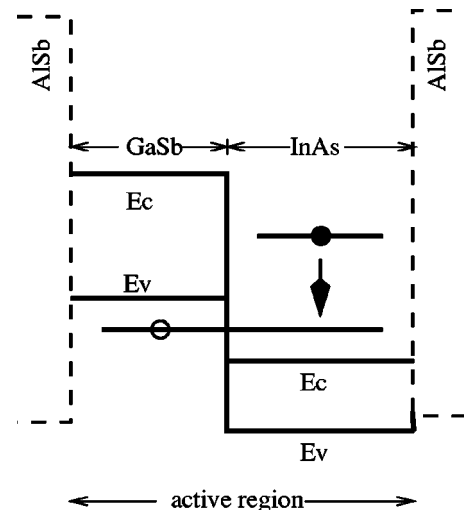


FIG. 1. The possible hybridization between the InAs conduction band states and the GaSb valence band states in the active region of a broken gap quantum well structure provides infrared radiation.

large amplitude in the InAs layer. On the other hand, to drain the electrons out of the hybridized state in order to achieve population inversion for lasing, the wave function should have a large component from the GaSb layer. A thorough understanding of this hybridization is important not only for optoelectronic devices, but also for the fundamental theory of transport parallel to interfaces.

The optical property of a BGQW that is of most theoretical interest and most importance to optoelectronics involves the optical transition between these two levels. Hence, relevant issues to be studied are the dependence of the optical matrix elements on the degree of conduction-valence hybridization, tuning of the hybridization by varying the width of the GaSb layer, and the sensitivity of the quantized levels to this tuning. In this paper we will perform a theoretical calculation of the electronic structure and optical matrix elements in order to investigate these items. In Sec. II we present the model system we study and the basic assumptions in our theoretical calculation. Our results for the electronic structure and optical matrix elements are given in Sec. III and Sec. IV, respectively, and discussed in Sec. V.

II. MODEL AND THEORY

Our model system shown in Fig. 1 is a GaSb/InAs heterostructure sandwiched between two thick AlSb layers. The growth direction is [001] which defines the z axis. The x axis is along [100] and the y axis is along [010]. This system was studied earlier with a simple two-band model.²⁶ The essential feature of our model is the existence in the BGQW of quantized conduction band states in the InAs layer and hybridized quantum levels in the energy regime where the GaSb valence band overlaps with the InAs conduction band. Therefore, for simplicity we can assume that the two thick AlSb layers are bulk AlSb. As an illustration, one conduction band level and one hybridized level are plotted in Fig. 1. We will perform a band structure calculation for the BGQW shown in Fig. 1. The lattice constants are 6.096 Å for GaSb, 6.058 Å for InAs, and 6.136 Å for AlSb. With such a small lattice mismatch, the strain estimated from the deformation potential of these materials is not large enough to modify our conclusion qualitatively. Hence, in our theoretical calculation, strain will be neglected. As will be discussed in Sec. III, the essential feature of our model mentioned above and hence the conclusion reached by our calculation will remain intact even when this weak strain effect is taken into account.

We employ the effective bond orbital model²⁷ (EBOM) which is a tight-binding-like model defined on the Bravais lattice of the underlying crystal. The bases are constructed as linear combinations of orbitals centered on each lattice site having s or p symmetry, together with spin eigenstates. The basis functions constructed in this way diagonalize the spin-orbit interaction. Our model Hamiltonian includes local and nearest neighbor matrix elements. The degree of inversion asymmetry of the BGQW heterostructure under study is much higher than that of the individual InAs or GaSb constituent layers. Hence, in our calculation the effect of weak inversion symmetry is neglected for simplicity. On the other hand, the strong inversion symmetry of the BGQW and its combined effect with the spin-orbit coupling at finite in-plane wave vectors are fully taken into account in our theoretical treatment.

It is worthwhile to point out that the EBOM is not an atomistic model like the tight binding model. While the tight binding model is built from orbitals representing the degree of freedom of each individual atom, the bond orbitals in the EBOM are confined to a primitive unit cell and represent more than one atom. The symmetry of the EBOM is identical to that of the $\vec{k} \cdot \vec{p}$ model, and therefore in both models there is no asymmetry between the (110) and (1 $\bar{1}$ 0) directions. On the other hand, the difference between the EBOM and the $\vec{k} \cdot \vec{p}$ model is that the $\vec{k} \cdot \vec{p}$ model is a continuum model without a natural momentum cutoff, but the EBOM is discretized on the Bravais lattice of the crystal.

The bulk parameters of the EBOM, which are required for our calculation, are obtained by fitting the bulk band structure of the EBOM to that of the $\vec{k} \cdot \vec{p}$ Hamiltonian near the Γ point to the second order in k , as described in Ref. 27. The EBOM can therefore be considered as an effective mass theory discretized on the Bravais lattice. For small k vectors the two models are equivalent. However, since the EBOM is discretized on the Bravais lattice, it gives better results at large k . It is important to point out that usually, as in the present case, it is not even necessary to know the precise form of the effective bond orbitals.

Because of the large overlap between the InAs conduction band and the GaSb valence band, the split-off band must be included in our treatment. Hence, we will deal with essentially an eight-band Kane model. We consider BGQW heterostructures grown in the [001] direction, with n labeling the (001) planes. Then the position of a lattice site \vec{R}_n in the n th plane can be expressed as $(na/2, \vec{R}_n)$, where a is the lattice constant of the conventional unit cell. The eight-bond orbitals at each lattice site are conventionally labeled as $(S_{\frac{1}{2}\frac{1}{2}})$, $(S_{\frac{1}{2}} - \frac{1}{2})$, $(P_{\frac{3}{2}\frac{3}{2}})$, $(P_{\frac{3}{2}\frac{1}{2}})$, $(P_{\frac{3}{2}} - \frac{1}{2})$, $(P_{\frac{3}{2}} - \frac{3}{2})$, $(P_{\frac{1}{2}\frac{1}{2}})$, and $(P_{\frac{1}{2}} - \frac{1}{2})$. We denote by $|n, \vec{R}_n, \alpha\rangle$ the α th bond orbital at position $(na/2, \vec{R}_n)$. In terms of these bond orbitals, we define a basis set of planar orbitals

$$|n, \vec{k}_{\parallel}, \alpha\rangle = N_{\parallel}^{-1/2} \sum_{\vec{R}_n} \exp(i\vec{k}_{\parallel} \cdot \vec{R}_n) |n, \vec{R}_n, \alpha\rangle, \quad (1)$$

where \vec{k}_{\parallel} is an in-plane wave vector, and N_{\parallel} is the number of sites in each plane.

Using this basis of planar orbitals, the Hamiltonian

$$H = \sum_{\vec{k}_{\parallel}} H_{\vec{k}_{\parallel}}$$

is decomposed into a linear combination of partial Hamiltonians $H_{\vec{k}_{\parallel}}$. The partial Hamiltonian

$$H_{\vec{k}_{\parallel}} = \sum_{n\alpha\beta} e_{n, \vec{k}_{\parallel}, \alpha\beta} |n, \vec{k}_{\parallel}, \alpha\rangle \langle n, \vec{k}_{\parallel}, \beta| + \sum_{n\alpha\beta} (v_{n, \vec{k}_{\parallel}, \alpha\beta} |n+1, \vec{k}_{\parallel}, \alpha\rangle \langle n, \vec{k}_{\parallel}, \beta| + \text{H.c.}) \quad (2)$$

TABLE I. Parameters used to determine effective bond orbital parameters.

	InAs	GaSb	AlSb
a (Å)	6.0583	6.082	6.133
E_g (eV)	0.41	0.8128	2.32
m_c/m_0	0.024	0.042	0.18
Δ (eV)	0.38	0.752	0.75
E_p (eV)	22.2	22.4	18.7
γ_1	19.67	11.80	4.15
γ_2	8.37	4.03	1.01
γ_3	9.29	5.26	1.75

is diagonal with respect to the in-plane wave vectors \vec{k}_{\parallel} , and block tridiagonal with respect to the remaining quantum numbers. This form of Hamiltonian is suitable for numerical computations.

The matrix elements in $H_{\vec{k}_{\parallel}}$, except for those $v_{n,\vec{k}_{\parallel},\alpha\beta}$ that connect the two bond orbital planes forming an interface, are set to the values for the corresponding bulk materials. At an interface, we follow the commonly accepted approach of determining the value of $v_{n,\vec{k}_{\parallel},\alpha\beta}$ as the average of the parameter values of the bulk materials on each side of the interface. The material parameter values from which the effective bond orbital parameters are derived are given in Table I. The valence band offsets are 0.56 eV for GaSb-InAs, 0.18 eV for AlSb-InAs, and -0.38 eV for AlSb-GaSb.

For a given \vec{k}_{\parallel} , the eight eigenfunctions

$$|\Psi_{\gamma,\vec{k}_{\parallel}}\rangle = \sum_{n,\alpha} F_{n,\vec{k}_{\parallel},\alpha}^{\gamma} |n,\vec{k}_{\parallel},\alpha\rangle; \quad \gamma=1,2,\dots,$$

and the corresponding band energies $E_{\gamma,\vec{k}_{\parallel}}$ can be readily obtained from Eq. (2) by diagonalizing a finite tridiagonal matrix for a BGQW of finite width. Knowing the eigensolutions, we will calculate the optical matrix elements.

The representation of the momentum operator in the bond orbital basis contains the leading local and nearest neighbor matrix elements. They are determined by mapping the bulk matrix elements to the $\vec{k} \cdot \vec{p}$ results up to and including terms linear in the wave vector.²⁸ In the planar orbital basis, its \vec{k}_{\parallel} -diagonal part can be expressed as

$$P^{\nu}(\vec{k}_{\parallel}) = \sum_{n\alpha\beta} P_{n,\vec{k}_{\parallel},\alpha\beta}^{\nu} |n,\vec{k}_{\parallel},\alpha\rangle \langle n,\vec{k}_{\parallel},\beta| \\ + \sum_{n\alpha\beta} (Q_{n,\vec{k}_{\parallel},\alpha\beta}^{\nu} |n+1,\vec{k}_{\parallel},\alpha\rangle \langle n,\vec{k}_{\parallel},\beta| + \text{H.c.}), \quad (3)$$

where $\nu = x,y,z$ is the polarization direction. The matrix elements are

$$P_{n,\vec{k}_{\parallel},\alpha\beta}^{\nu} = \sqrt{\frac{2}{m_0}} \langle n,\vec{k}_{\parallel},\alpha | p_{\nu} | n,\vec{k}_{\parallel},\beta \rangle, \quad (4)$$

$$Q_{n,\vec{k}_{\parallel},\alpha\beta}^{\nu} = \sqrt{\frac{2}{m_0}} \langle n+1,\vec{k}_{\parallel},\alpha | p_{\nu} | n,\vec{k}_{\parallel},\beta \rangle, \quad (5)$$

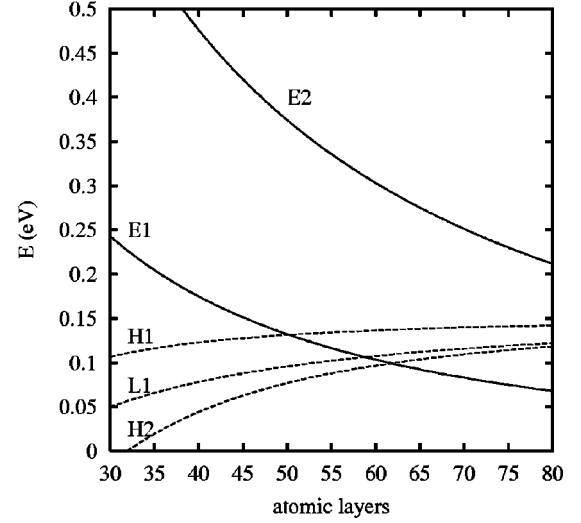


FIG. 2. Electron energies in an AlSb-InAs-AlSb quantum well (solid curves) and in an AlSb-GaSb-AlSb quantum well (dashed curves) as functions of well width. All energies are measured from the InAs conduction band edge.

where m_0 is the free electron mass. In the above matrix elements we have included the prefactor $\sqrt{2}/m_0$ so that these matrix elements have units $(\text{eV})^{1/2}$.

III. ELECTRONIC STRUCTURE

In the following we will examine the electronic structure of the InAs-GaSb BGQW shown in Fig. 1. Before the InAs layers and the GaSb layers are coupled together, we will denote the n th electronic levels in the conduction band by En , the n th energy levels in the heavy-hole band by Hn , and the n th energy levels in the light-hole band by Ln . Such conventional labeling is unambiguous for $\vec{k}_{\parallel} = \vec{0}$.

The symmetry properties of the EBOM at $\vec{k}_{\parallel} = 0$ allow the conduction band states in the InAs layers to hybridize with the light-hole band states in the GaSb layers, but not with the heavy-hole band states. We would like first to locate the region of the BGQW structure in which we can fine tune the degree of such hybridization. For this purpose, we perform two energy level calculations; one with zero InAs layer width and the other with zero GaSb layer width. The results are plotted in Fig. 2 as functions of the number of atomic layers. We see that for 58 atomic layers, the GaSb $L1$ level overlaps with the InAs $E1$ level. Hence, the region around 60 atomic layers will be the reasonable starting BGQW structure for tuning the system into maximum hybridization. We should be aware of the fact that different confinement boundary conditions also affect the degree of hybridization, as will be seen in our computed results below.

We will set 60 atomic layers for the InAs constituent and vary the GaSb width from 30 to 80 atomic layers. In the absence of interface coupling, the $H1$, $E1$, $H2$, and $L1$ levels at $\vec{k}_{\parallel} = \vec{0}$ are shown in Fig. 3 as dashed curves (hole states are the same as in Fig. 2). In the BGQW sample with 80 atomic layers of GaSb, these four levels are ordered as $H1 > L1 > H2 > E1$. When the interface coupling is turned on, these four levels are shown in Fig. 3 as solid curves. For convenience of description, we use the results at

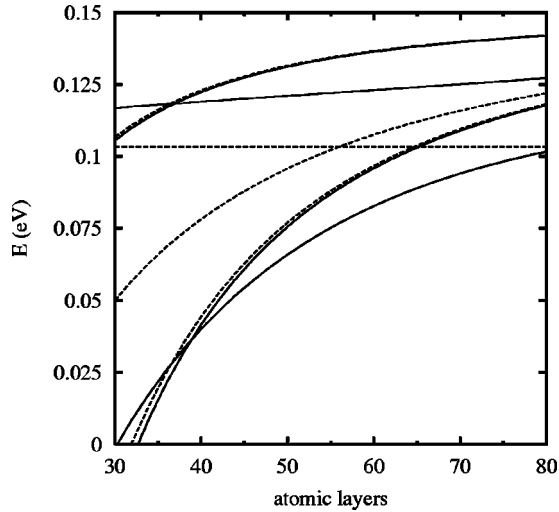


FIG. 3. Zone center ($\vec{k}_{\parallel} = 0$) $H1$, $H2$, $L1$, and $E1$ levels as functions of GaSb layer width in an InAs-GaSb BGQW with 60 InAs atomic layers. Dashed curves are for the case without InAs-GaSb interface coupling (ordered as $H1 > L1 > H2 > E1$ at 80 atomic layers of GaSb), and the solid curves are for the case with the InAs-GaSb interface coupling (for convenience, ordered as $H1 > E1 > H2 > L1$ at 80 atomic layers of GaSb).

80 atomic layers of GaSb to label them as $H1 > E1 > H2 > L1$. Because of the symmetry properties at $\vec{k}_{\parallel} = \vec{0}$, the conduction band states have negligible influence on $H1$ and $H2$ levels. The heavy-hole levels are only slightly perturbed by the change of boundary conditions. On the other hand, the $L1$ and $E1$ levels are strongly hybridized and repel each other. The difference between the solid curves and the dashed curves is also due to the different confinement boundary conditions as mentioned above. In the region of GaSb width between 50 and 60 atomic layers, the separation of the two resulting hybridized levels is about 40–55 meV.

To demonstrate the spatial properties of hybridized states, we have calculated the real space occupation probability

$$\mathcal{O}_n^{\gamma}(\vec{k}_{\parallel} = \vec{0}) \equiv \sum_{\alpha} |F_{n, \vec{k}_{\parallel} = \vec{0}, \alpha}^{\gamma}|^2; \quad \gamma = 1, 2, \dots$$

$\mathcal{O}_n^{\gamma}(\vec{k}_{\parallel} = \vec{0})$ values of five eigenstates in a BGQW with 56 GaSb atomic layers and 60 InAs atomic layers are plotted in Fig. 4. From top to bottom, the first state is $E2$, which is largely confined in the InAs layers. The second and fourth states, which are localized in GaSb layers, are $H1$ and $H2$, respectively. The third and the lowest states are $E1$ - $L1$ hybridized states. To be consistent with our earlier convention, the third state is $E1$, and the lowest state is $L1$. One way to further analyze this issue is to decompose the total occupation probability into a partial occupation probability for each α band. Such a decomposition is shown in Fig. 5 with dotted curves for the $E1$ state, and solid curves for the $L1$ state. In this figure, the two upper plots are for the $P_{3/2, \pm 1/2}$ components and the two lower plots are for the $S_{1/2, \pm 1/2}$ components. We see that the tail of the $E1$ (or $L1$) state in the GaSb (or InAs) region has the same component profile as its main part in the InAs (or GaAs) region. Such features were also obtained for InAs-GaSb superlattices in Ref. 25.

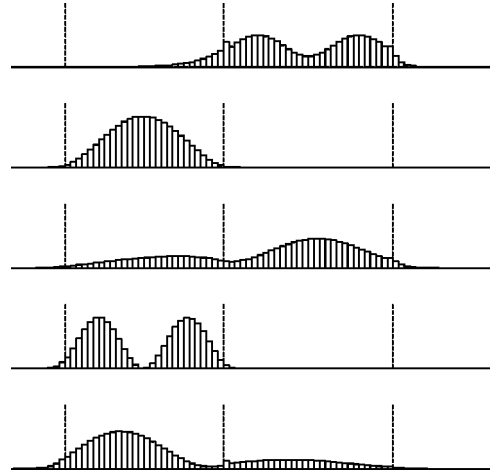


FIG. 4. Real space occupation probability of five zone center ($\vec{k}_{\parallel} = 0$) eigenstates in the active region of a BGQW with 56 GaSb atomic layers and 60 InAs atomic layers.

In our derivation of the eigensolutions for a BGQW heterostructure, the effect of strain has been neglected. The separations between the eigenenergies so-obtained for $\vec{k}_{\parallel} = \vec{0}$, which are determined by the confinement potential, are substantially larger than the energy shifts produced by the strain. Hence, even if the effect of strain is included in an improved calculation, the formation of $E1$ - $L1$ hybridized states is still dominated by the confinement potential, and the degree of hybridization can still be tuned by changing the width of the GaSb and/or the InAs layers. In this respect, the conclusion reached with our present calculation will remain intact when the effect of strain is taken into account.

An interesting question is, when a charge carrier occupies an $E1$ - $L1$ hybridized state, will its physical properties be electronlike or holelike? For example, what will be the cyclotron effective mass of such a charge carrier? One relevant quantity is the probability

$$\mathcal{O}_{\text{InAs}}^{\gamma}(\vec{k}_{\parallel} = \vec{0}) \equiv \sum_{n \in \text{InAs}} \mathcal{O}_n^{\gamma}(\vec{k}_{\parallel} = \vec{0}); \quad \gamma = 1, 2, \dots,$$

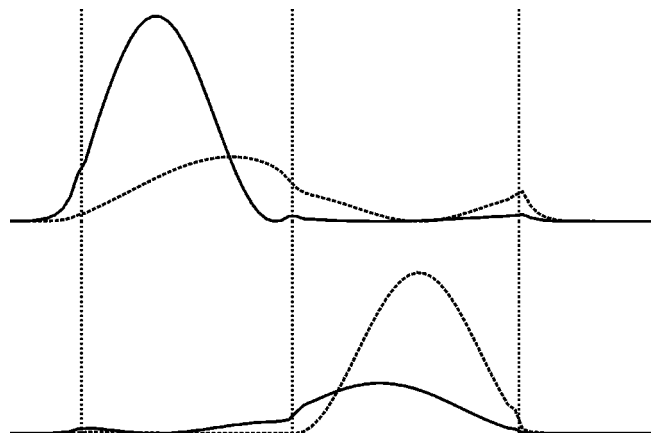


FIG. 5. Structure of the states $L1$ (solid curves) and $E1$ (dotted curves), with the two upper plots for the $P_{3/2, \pm 1/2}$ components and the two lower plots for the $S_{1/2, \pm 1/2}$ components.

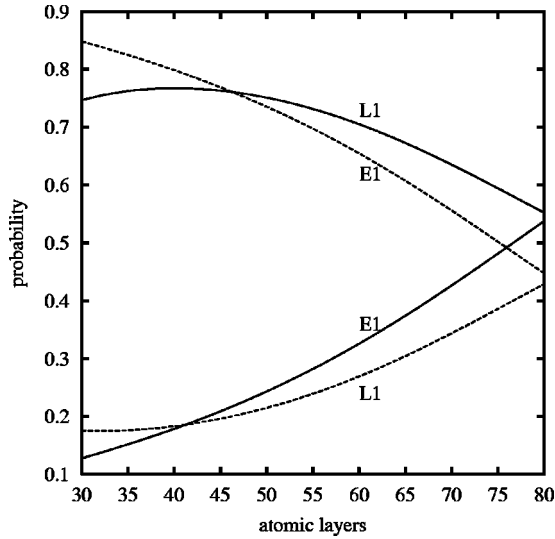


FIG. 6. Probabilities of finding an electron in the GaSb layers (solid lines) or in the InAs layers (dashed lines) as a function of GaSb layer width, when the electron occupies the hybridized states $E1$ or $L1$ in a BGQW with 60 InAs atomic layers.

of finding the electron in InAs layers when it occupies the γ th eigenstate. For the two hybridized states (labeled as $E1$ and $L1$ in our convention) in an InAs-GaSb BGQW with 56 InAs atomic layers, the results are plotted in Fig. 6 as a function of the number of GaSb atomic layers. The solid curves are for $\mathcal{O}_{\text{GaSb}}^\gamma(\vec{k}_\parallel = \vec{0})$, and the dashed curves are for $\mathcal{O}_{\text{InAs}}^\gamma(\vec{k}_\parallel = \vec{0})$. For thin GaSb layers, the charge carrier in a hybridized state is mostly either electronlike or holelike. However, as the width of the GaSb layers increases toward 80 atomic layers, the characteristic features of the charge carrier remain to be studied.

The above calculations for zone center ($\vec{k}_\parallel = 0$) states are repeated for finite \vec{k}_\parallel , and the dispersion relations of various subbands are shown in Fig. 7 for a BGQW with 60 InAs atomic layers and 60 GaSb atomic layers. We have chosen \vec{k}_\parallel along the $[100]$ direction, or the x axis. At zone center, from top to bottom the levels are $E2$, $H1$, $E1$, $H2$, $L1$, and $L2$. In the region of finite \vec{k}_\parallel , the spin splitting of levels and the anticrossing of levels are clearly seen. We will return to these dispersion relations later for further discussion.

We have mentioned that our BGQW system was studied earlier with a simple two-band model,²⁶ where only the $H1$ and the $E1$ levels are included. Therefore, in Ref. 26 there is no $E1$ - $L1$ hybridization. The energy bands shown in Fig. 2 of Ref. 26 correspond to our $E1$ and $H1$ bands in Fig. 7, within the region $0 < ka < 0.12$. The two-band calculation does yield an anticrossing at finite \vec{k}_\parallel , but gives no spin-orbit splitting.

IV. OPTICAL MATRIX ELEMENTS

Knowing the eigenfunctions of the BGQW heterostructure, the optical matrix elements are readily calculated with Eq. (3). Because for finite \vec{k}_\parallel each dispersion curve is spin-orbit split into two curves, we distinguish them as Ena and Enb for conduction band states, Hna and Hnb for heavy-

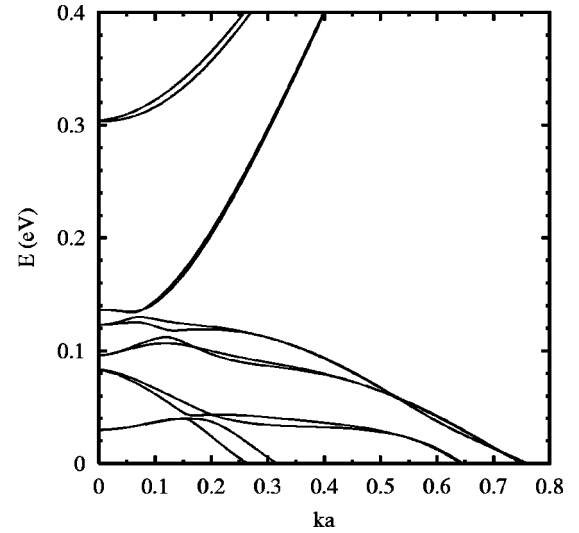


FIG. 7. Subband dispersion with \vec{k}_\parallel along the $[100]$ direction for an InAs-GaSb BGQW with 60 InAs atomic layers and 60 GaSb atomic layers.

hole band states, and Lna and Lnb for light-hole band states. For convenience, in the region of small \vec{k}_\parallel , the lower spin-orbit split dispersion curve is assigned a and the higher one with b .

There are numerous optical transitions between each pair of states for different polarizations of the electromagnetic waves. The selection rules are complicated by the anticrossing of levels as well as the hybridization between InAs conduction band states and GaSb valence band states. Hence, here our study will focus on the cases of our interest: the optical transitions from the $E2a$ and $E2b$ levels to the $E1a$, $E1b$, $H1a$, and $H1b$ levels. As will be discussed later, such transitions are relevant to possible infrared lasers based on BGQW heterostructures. We would like to mention that parallel to our work, in Ref. 25, the optical transition matrix elements at $\vec{k}_\parallel = 0$ with in-plane polarization in InAs-GaSb superlattices were studied as functions of the superlattice period.

By analyzing our extensive numerical results, we have reached the following selection rules for transitions from the $E2a$ and $E2b$ levels to the $E1a$, $E1b$, $H1a$, and $H1b$ levels. For \vec{k}_\parallel in the $[100]$ or $[110]$ direction, among the two transitions from $E2a$ (or $E2b$) to $E1a$ or $E1b$, only one is allowed. Similarly, among the two transitions from $E2a$ (or $E2b$) to $H1a$ or $H1b$, only one is allowed. However, if \vec{k}_\parallel is along a low symmetry direction in the two-dimensional Brillouin zone, such as $[210]$ for example, all transitions are allowed. It is worthwhile to point out that these selection rules for a BGQW, which is asymmetric, happen to be the same as the selection rules for the intersubband transitions in a symmetric conduction band quantum well, derived with a simplified eight-band model.²⁹

The numerical results to be discussed below were obtained for a BGQW with 60 InAs atomic layers and 60 GaSb atomic layers, the band structure of which is given in Fig. 7. From Fig. 6 we see a significant $E1$ - $L1$ hybridization in this BGQW heterostructure. The square of the amplitude of optical matrix elements with z polarization is shown in Fig. 8.

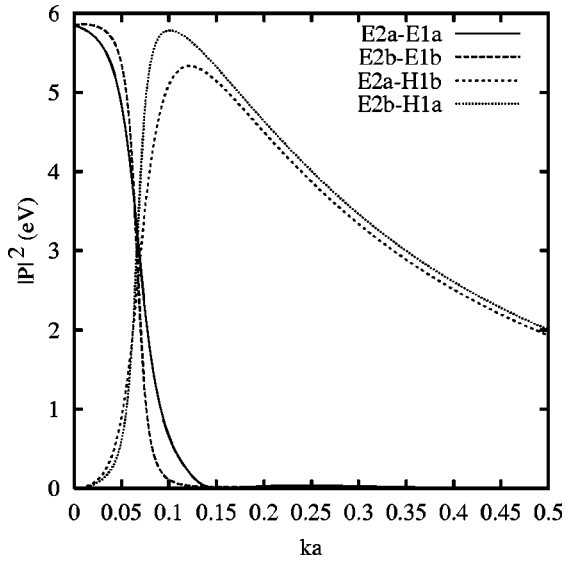


FIG. 8. Square of the amplitude of optical matrix elements with z polarization as functions of \vec{k}_{\parallel} , which is along the x axis, for a BGQW with 60 InAs atomic layers and 60 GaSb atomic layers.

At $\vec{k}_{\parallel} = 0$, the optical matrix element is zero for the $E2 \rightarrow H1$ transition, but is large for the $E2 \rightarrow E1$ transition, as expected from the symmetry properties. As \vec{k}_{\parallel} increases, the anticrossing between the $E1$ band and the $H1$ band occurs around $\vec{k}_{\parallel} a \approx 0.75$. Consequently, the $E2 \rightarrow E1$ transition drops sharply to zero, while the $E2 \rightarrow H1$ transition picks up strength rapidly.

By changing the polarization of the electromagnetic wave and repeating the calculations for optical matrix elements, the results for y polarization are shown in Fig. 9 and for x polarization in Fig. 10. The strengths of these transitions are substantially smaller than those for the z polarization, by about two orders of magnitude. The strong wave vector dependence of the optical matrix elements in Figs. 9 and 10 is due to the combined effect of spin-orbit splitting and anticrossing of energy bands. The drastic difference between the curves in Fig. 9 and the corresponding curves in Fig. 10

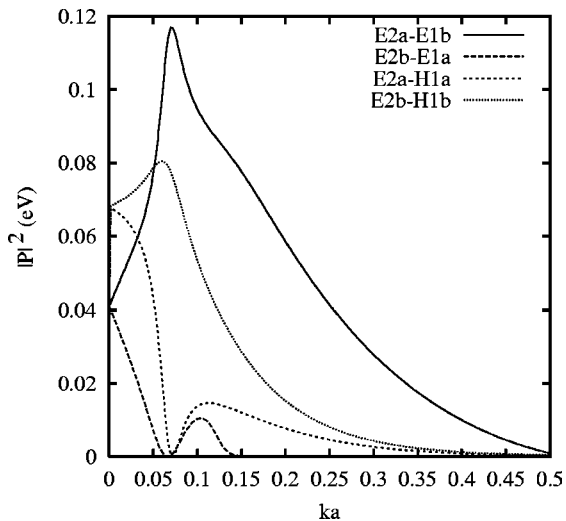


FIG. 9. Same as Fig. 8 but with y polarization of the electromagnetic wave.

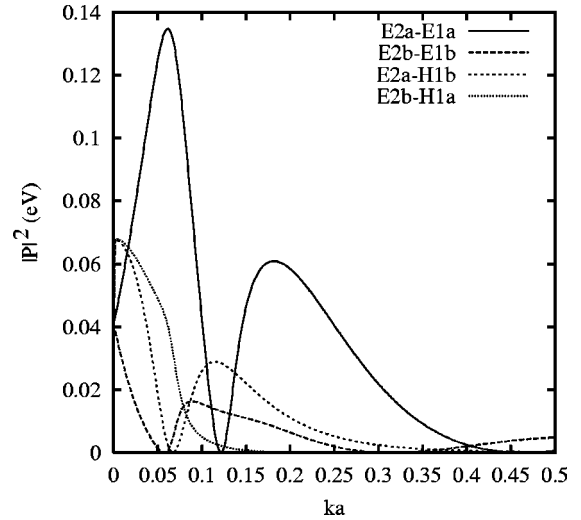


FIG. 10. Same as Fig. 8 but with x polarization of the electromagnetic wave.

indicates the strong anisotropy of the optical matrix elements with respect to in-plane polarization.

V. DISCUSSION

The very unusual feature of the BGQW heterostructures is the eigenstates formed by the hybridization of conduction band states at one side of the interface with valence band states at the other side. We made a thorough investigation of the formation of such states and their influence on the optical properties of a BGQW. However, their influence on the transport properties parallel to the interfaces is perhaps a more important issue for fundamental study. If one tunes the system to have the Fermi energy lying in a conduction-valence hybridized two-dimensional energy band, depending on the degree of hybridization, the parallel transport properties can change from completely electronlike to complete holelike.

Another relevant issue for fundamental study is the spin-orbit splitting. Recently, there has been much interest in the effect of spin-orbit interactions in two-dimensional electron gases. For example, Shubnikov-de Haas measurements of spin-orbit splitting have been performed on symmetric InAs/GaSb quantum wells³⁰ and on symmetric InAs/AlSb quantum wells,³¹ in which the origin of spin-orbit interaction is the lack of inversion symmetry in the bulk crystal structure. Because of the asymmetry of the BGQW itself, very large spin-orbit splittings appear in the energy bands as shown in Fig. 7. Consequently, BGQW heterostructures are good candidates for investigating phenomena that are related to spin-orbit interaction.

BGQW heterostructures have great potential in technological applications for lasers and detectors tunable in infrared wavelengths.^{32,33} Our calculations can serve as the theoretical model for such infrared lasers. To make a bipolar laser similar to conventional quantum lasers, in Fig. 1 the AlSb layers at the InAs side should be n doped, and the AlSb layers at the GaSb side should be p doped. The number of InAs atomic layers should be around 60, and the number of GaSb atomic layers should be between 70 and 80. Then, from Fig. 6 we see a strong $E1-L1$ hybridization. By adjust-

ing the acceptor concentration, we can set the Fermi level between the $E1$ level and the $H2$ level shown in Fig. 4. When such a BGQW heterostructure is connected to an external circuit, electrons that are injected into the $E2$ energy band will relax to the zone center and make radiation transitions to the $E1$ band due to the large optical matrix elements of z -polarized light. Then the strong conduction-valence hybridization of the $E1$ band states provides rapid draining of electrons from the $E1$ band into the external circuit via the GaSb valence band states. From Fig. 7 we estimate the energy of the emitted photons to be 0.18–0.2 eV, corresponding to a wavelength of about $6 \mu\text{m}$. Around this wavelength there exist infrared windows, and consequently such radiation source will be extremely useful.

To close this paper, we must mention the work of Ref. 25, in which the electronic structure and optical matrix elements at the zone center ($\vec{k}_{\parallel} = 0$) of InAs-GaSb superlattices were calculated with both a plane wave pseudopotential method and the eight-band $\vec{k} \cdot \vec{p}$ method. In that paper the effects of

the superlattice period on various physical quantities at the zone center were studied in detail. In particular, the authors of Ref. 25 found a zone center $E1$ - $H1$ coupling manifested by band anticrossing at superlattice period $n = 28$, as well as a zone center $L1$ - $H2$ coupling and anticrossing around $n = 13$. Such features are absent in the $\vec{k} \cdot \vec{p}$ method because it fails to recognize the atomistic details in no-common-atom superlattices. How these features will affect the two-dimensional dispersion relation quantitatively, and hence our results for the formation of $E1$ - $L1$ hybridization and the in-plane physical properties of a single BGQW heterostructure, as well as their impact on the theoretical modeling of infrared lasers and detectors, remain open questions.

ACKNOWLEDGMENT

This work was supported by the Norwegian Research Council (NFR) under Grant No. 111071/431.

-
- *Present address: Alcatel Space Norway AS, P.O. Box 138, N-3191 Horten, Norway.
- ¹H. Munekata, J. C. Maan, L. L. Chang, and L. Esaki, *J. Vac. Sci. Technol. B* **5**, 809 (1987).
 - ²G. Tuttle, H. Kroemer, and J. H. English, *J. Appl. Phys.* **65**, 5239 (1989); P. F. Hopkins, A. J. Rimberg, R. M. Westervelt, G. Tuttle, and H. Kroemer, *Appl. Phys. Lett.* **58**, 1428 (1991); Ikai Lo, W. C. Mitchel, M. O. Manasreh, C. E. Stutz, and K. R. Evans, *ibid.* **60**, 751 (1992); J.-P. Cheng, Ikai Lo, and W. C. Mitchel, *J. Appl. Phys.* **76**, 667 (1994); Ikai Lo, W. C. Mitchel, S. Elhamri, R. S. Newrock, and R. Kaspi, *Appl. Phys. Lett.* **65**, 1024 (1994).
 - ³T. P. Smith III, H. Nunekata, L. L. Chang, F. F. Fang, and L. Esaki, *Surf. Sci.* **196**, 687 (1998); Ikai Lo, W. C. Mitchel, and J.-P. Cheng, *Phys. Rev. B* **48**, 9118 (1993).
 - ⁴J. Kono, B. D. McCombe, J.-P. Cheng, Ikai Lo, W. C. Mitchel, and C. E. Stutz, *Phys. Rev. B* **50**, 12 242 (1994); J.-P. Cheng, J. Kono, B. D. McCombe, Ikai Lo, W. C. Mitchel, and C. E. Stutz, *Phys. Rev. Lett.* **74**, 450 (1995).
 - ⁵M. Sweeny and J. Xu, *Appl. Phys. Lett.* **54**, 546 (1989).
 - ⁶J. R. Söderström, D. H. Chow, and T. C. McGill, *Appl. Phys. Lett.* **55**, 1094 (1989).
 - ⁷L. F. Luo, R. Beresford, and W. I. Wang, *Appl. Phys. Lett.* **55**, 2023 (1989).
 - ⁸R. Beresford, L. F. Luo, and W. I. Wang, *Appl. Phys. Lett.* **56**, 551 (1990).
 - ⁹R. Beresford, L. F. Luo, K. F. Longenbach, and W. I. Wang, *Appl. Phys. Lett.* **56**, 952 (1990).
 - ¹⁰D. A. Collins, E. T. Yu, Y. Rajakarunayake, J. R. Söderström, D. Z.-Y. Ting, D. H. Chow, and T. C. McGill, *Appl. Phys. Lett.* **57**, 683 (1990).
 - ¹¹D. Z.-Y. Ting, D. A. Collins, E. T. Yu, D. H. Chow, and T. C. McGill, *Appl. Phys. Lett.* **57**, 1257 (1990).
 - ¹²L. Yang, J. F. Chen, and A. Y. Cho, *J. Appl. Phys.* **68**, 2997 (1990).
 - ¹³D. Z.-Y. Ting, E. T. Yu, and T. C. McGill, *Phys. Rev. B* **45**, 3583 (1992).
 - ¹⁴E. E. Mendez, J. Nocera, and W. I. Wang, *Phys. Rev. B* **45**, 3910 (1992).
 - ¹⁵M. S. Kiledjian, J. N. Schulman, K. L. Wang, and K. V. Rousseau, *Phys. Rev. B* **46**, 16 012 (1992).
 - ¹⁶Maria A. Davidovich, E. V. Anda, C. Tejedor, and G. Platero, *Phys. Rev. B* **47**, 4475 (1993).
 - ¹⁷E. E. Mendez, H. Ohno, L. Esaki, and W. I. Wang, *Phys. Rev. B* **43**, 5196 (1991).
 - ¹⁸R. R. Marquardt, D. A. Collins, Y. X. Liu, D. Z.-Y. Ting, and T. C. McGill, *Phys. Rev. B* **53**, 13 624 (1996).
 - ¹⁹Y. X. Liu, R. R. Marquardt, D. Z.-Y. Ting, and T. C. McGill, *Phys. Rev. B* **55**, 7073 (1997).
 - ²⁰A. Zakharova, *J. Phys.: Condens. Matter* **11**, 4675 (1999).
 - ²¹Yia-Chung Chang and J. N. Schulman, *Phys. Rev. B* **31**, 2069 (1985).
 - ²²Ikai Lo, Jih-Chen Chiang, Shioh-Fon Tsay, W. C. Mitchel, M. Ahoujja, R. Kaspi, S. Elhamri, and R. S. Newrock, *Phys. Rev. B* **55**, 13 677 (1997).
 - ²³L.-W. Wang, S.-H. Wei, T. Mattila, A. Zunger, I. Vurgaftman, and J. R. Meyer, *Phys. Rev. B* **60**, 5590 (1999).
 - ²⁴R. Q. Yang and J. M. Xu, *Appl. Phys. Lett.* **59**, 181 (1991).
 - ²⁵H. Ohno, L. Esaki, and E. E. Mendez, *Appl. Phys. Lett.* **60**, 3153 (1992).
 - ²⁶Y. Naveh and B. Laikhtman, *Appl. Phys. Lett.* **66**, 1980 (1995).
 - ²⁷Y.-C. Chang, *Phys. Rev. B* **37**, 8215 (1988).
 - ²⁸Y.-C. Chang, *J. Appl. Phys.* **68**, 4233 (1990).
 - ²⁹R. Q. Yang, J. M. Xu, and M. Sweeney, *Phys. Rev. B* **50**, 7474 (1994).
 - ³⁰J. Luo and P. J. Stiles, *Phys. Rev. B* **41**, 7685 (1990).
 - ³¹J. P. Heida, B. J. van Wees, J. J. Kuipers, and T. M. Klapwijk, *Phys. Rev. B* **57**, 11 911 (1998).
 - ³²R. M. Biefeld, A. A. Allerman, and S. R. Kurtz, *Mater. Sci. Eng., B* **51**, 1 (1998).
 - ³³J. R. Meyer, L. J. Olafsen, E. H. Aifer, W. W. Bewley, C. L. Felix, I. Vurgaftman, M. J. Yang, L. Goldberg, D. Zhang, C. H. Lin, S. S. Pei, and D. H. Chow, *IEE Proc.: Optoelectron.* **145**, 275 (1998).